Thermal Prestress in Composite Compliant Shell Mechanisms (DETC2018-85826)

Jonathan P. Stacey, Matthew P. O'Donnell, Mark Schenk
Bristol Composites Institute (ACCIS)
Department of Aerospace Engineering
University of Bristol
Bristol, BS8 1TR, United Kingdom
Email: jonathan.stacey@bristol.ac.uk

ABSTRACT

This paper explores the ability to tailor the mechanical properties of composite compliant shell mechanisms, by exploiting the thermal prestress introduced during the composite laminate cure. An extension of an analytical tape spring model with composite thermal analysis is presented, and the effect of the thermal prestress is studied by means of energy landscapes for the cylindrical composite shells. Tape springs that would otherwise be monostable structures become bistable and exhibit greater ranges of low-energy twisting with thermally-induced prestress. Predicted shell geometries are compared with finite element results and manufactured samples, showing good agreement between all approaches. Wider challenges around the manufacture of prestressed composite compliant mechanisms are discussed.

1 Introduction

Compliant shell mechanisms are thin shell structures capable of large deflections, for small strain elastic deformations. In addition to enabling tailored force and displacement responses, a significant advantage of such mechanisms is the lack of need for mechanical joints, in turn removing friction and reducing maintenance requirements. While the design of compliant mechanisms has been studied for isotropic materials [1, 2], composite materials offer further benefits and opportunities to the mechanism designer. These include high specific properties, anisotropic deformation behaviour, ease of manufacturing complex geometries, and alternative methods of tailoring the residual stress state of the mechanism. This study aims to investigate the effects of thermal prestress, arising from mismatches in thermal expansion coefficients, on the behaviour of composite tape springs. The magnitude of the thermal prestress can be tailored through the composite laminate layup [3]. Tape springs are a class of structures that have been investigated previously as compliant mechanisms [4, 5], and have demonstrated bistability [6] and zero stiffness capabilities [5, 7, 8]. In classical mechanisms multiple members would be required to enable such behaviour [9–11]. This work uses the analytical model by Guest and Pellegrino [4], which assumes that the tape spring is kinematically constrained to the surface of an underlying cylinder. The model is extended by incorporating the thermal prestress introduced in composite laminate materials, and it is demonstrated that the extended tape spring model correlates well with FE models and manufactured samples. The feasibility of creating zero torsional stiffness composite tape springs is briefly explored mathematically.

In addition to geometric and material considerations, the design space for compliant mechanisms also includes residual stress states. Residual thermal stress due to composite manufacturing has been subject of extensive research efforts, and often aims to describe localised thermal effects and warping in detail [12]. However, for the work presented in this paper Classical Laminate Analysis (CLA), *e.g.* [13], provides a sufficiently accurate model of composite thermal behaviour. Laminates with non-symmetrical layups often exhibit warp due to the mismatch between thermal expansion coefficients between plies, and as such are often deliberately avoided [14]. However, these thermal effects can be used to provide prestress [15], to obtain desirable behaviour in tape springs and other thin shell structures [16–18]. Viscoelastic effects also affect the prestress [19–21], but are beyond the scope of this work.

This paper aims to evaluate the potential of using thermal prestress in the design of stiffness-tailored composite compliant shell mechanisms. Specifically, the focus is on reducing torsional stiffness within composite tape springs and evaluating

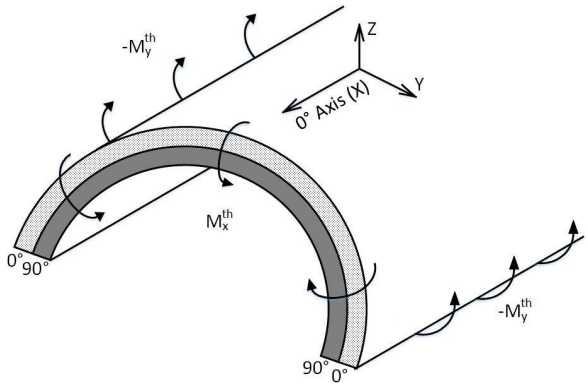

Fig. 1: Post-cure thermal strains produce a 'coiling-up' moment, M_x^{th}, in the longitudinal direction, and an 'opening-out' moment, M_y^{th}, in the hoop direction

Table 1: Material Data IM7-8552

$E_{11} = 161$ GPa	$\alpha_{11} = -0.1 \cdot 10^{-6}$ K^{-1}
$E_{22} = 11.38$ GPa	$\alpha_{22} = 31 \cdot 10^{-6}$ K^{-1}
$G_{12} = 5.17$ GPa	$t = 0.131$ mm
$\nu_{12} = 0.32$	$\rho = 1.57 \cdot 10^{3}$ kg/m^3

the feasibility of zero torsional stiffness prestressed composite shell structures. Such compliant mechanisms have potential for applications in medical exoskeletons [22], deployable spacecraft structures [23], and morphing aerostructures [18].

The paper is structured as follows. First, the extended analytical formulation is presented, including rationale behind material selection, derivation of the strain energy equation and comparisons of energy landscapes and stability states. Next, two sections detail validation work: FE modelling and the manufacture of sample tape springs. The results of each approach are discussed and compared before final conclusions are presented.

2 Analytical Model

2.1 Material and Layup Selection

To ascertain the potential of thermally prestressed composite compliant mechanisms, a layup and material configuration was selected which would exhibit the maximum thermally-induced bending moments per unit thickness. A cross-ply laminate configuration – where the fibres in the bottom half of the laminate lie perpendicular to those in the upper half – was therefore selected. This provides the greatest overall mismatch of thermal expansion coefficients through the laminate thickness. Wider ranges of composite laminate layups are beyond the scope of the current work.

Tape springs were chosen as a representative compliant shell mechanism due to their ease of manufacture and well-understood mechanical behaviour. By placing fibres at 90° to the longitudinal axis on the inner surface of the tape spring (*i.e.* $[90_N/0_N]$, where N represents the number of plies) the bending moments produced upon cooling will be similar to those produced by mechanically prestressed isotropic tape springs [5]. The thermal strains in such cross-ply laminates produce a 'coiling-up' moment, M_x^{th}, in the longitudinal direction, and an 'opening-out' moment, M_y^{th}, in the hoop direction (see Figure 1). Carbon fibre composites were chosen due to their high specific stiffness and low creep characteristics relative to glass and aramid fibre reinforcements, as well as its suitable thermal expansion properties. Hexcel IM7-8552 was used as a benchmark composite material due to its general availability and well-characterised properties [24]; see Table 1.

2.2 Elastic Strain Energy

In this work, the effect of thermal prestress on the energy landscape of anisotropic composite tape springs is considered. Following the approach of Guest and Pellegrino [4], the strain energy per unit area, U, stored in the tape spring is

$$U = \frac{1}{2}(\Delta\boldsymbol{\kappa}^T \mathbf{D}^* \Delta\boldsymbol{\kappa}), \tag{1}$$

where $\mathbf{D}^*$ is the reduced bending stiffness matrix

$$\mathbf{D}^* = \mathbf{D} - \mathbf{B}^T\mathbf{A}^{-1}\mathbf{B}, \tag{2}$$

and **A**, **B** and **D** are the in-plane, coupling and bending stiffness matrices of Classical Laminate Analysis (CLA) [13]. The $\mathbf{D}^*$ matrix accounts for the contribution of non-zero **B** matrices to the strain energy.

The strain energy equation is non-dimensionalised as

$$\hat{U} = U\frac{R^2}{D_{11}^*}, \tag{3}$$

using the manufacture tooling radius, R, and the reduced bending stiffness term, D_{11}^* [4].

In the Guest and Pellegrino model, an inextensional tape spring shell element (with existing curvature κ_y) is rotated around an underlying cylinder to investigate the curvature changes, $\Delta\boldsymbol{\kappa}$, that occur during twist. The modification made in this work is that change in curvature,

$$\Delta\boldsymbol{\kappa} = \boldsymbol{\kappa}_{\text{cylinder}} - \boldsymbol{\kappa}_{\text{warped}}, \tag{4}$$

is measured with respect to a thermally-warped element with curvatures $\boldsymbol{\kappa}_{\text{warped}}$, rather than an element with only manufactured curvature κ_y. Thus, the strain energy calculated will be that required to conform the warped element to the underlying cylinder ($\boldsymbol{\kappa}_{\text{cylinder}}$).

The curvature of the tape spring on the underlying cylinder is based on a Mohr's circle of curvature

$$\boldsymbol{\kappa}_{\text{cylinder}} = \frac{C}{2}\begin{bmatrix} 1-\cos(2\theta) \\ 1+\cos(2\theta) \\ 2\sin(2\theta) \end{bmatrix}, \tag{5}$$

where θ refers to the twist angle, and C the curvature of an underlying cylinder [5]. For this model to remain valid, the post-cure tape spring geometry must approximately conform to an underlying cylinder.

The curvature of the thermally warped tape spring (*i.e.* the origin state) is defined as

$$\boldsymbol{\kappa}_{\text{warped}} = \begin{bmatrix} 0 \\ 1/R \\ 0 \end{bmatrix} + \Delta\boldsymbol{\kappa}^{th}, \tag{6}$$

where the thermal curvature changes during cooling from manufacture, $\Delta\boldsymbol{\kappa}^{th}$ are added to the manufacture tooling radius.

The changes in curvature of an anisotropic plate due to thermally-induced bending moments ($\mathbf{M}^{th}$) and in-plane forces ($\mathbf{N}^{th}$) [25] can be evaluated as

$$\Delta\boldsymbol{\kappa}^{th} = \begin{bmatrix} \Delta\kappa_x^{th} \\ \Delta\kappa_y^{th} \\ \Delta\kappa_{xy}^{th} \end{bmatrix} = \Delta T(\mathbf{D}^*)^{-1}(\mathbf{M}^{th} - \mathbf{B}\mathbf{A}^{-1}\mathbf{N}^{th}). \tag{7}$$

The thermal moments $\mathbf{M}^{th}$ and in-plane forces $\mathbf{N}^{th}$ per degree Celsius [26] are given as

$$\mathbf{M}^{th} = \begin{bmatrix} M_x^{th} \\ M_y^{th} \\ M_{xy}^{th} \end{bmatrix} = \frac{H^2}{8}\begin{bmatrix} W_2^{th}\xi_5 \\ -W_2^{th}\xi_5 \\ W_2^{th}\xi_7 \end{bmatrix}, \tag{8}$$

and

$$\mathbf{N}^{th} = \begin{bmatrix} N_x^{th} \\ N_y^{th} \\ N_{xy}^{th} \end{bmatrix} = \frac{H}{2}\begin{bmatrix} W_1^{th} + W_2^{th}\xi_1 \\ W_1^{th} - W_2^{th}\xi_1 \\ W_2^{th}\xi_3 \end{bmatrix}. \tag{9}$$

The ξ_i terms refer to lamination parameters [27], which allow the stiffness of any composite layup to be represented using at most 12 continuous parameters. Using this approach it is possible to gain physical insight into the underlying behaviour of the system without having to consider specific layups. In particular, using such an approach is valuable when trying to tailor designs to obtain an optimised configuration. For our investigation, the lamination parameter definitions can be conveniently rearranged,

$$\begin{aligned}
\xi_1 &= \frac{(A_{11}-A_{22})}{2W_2H},\\
\xi_3 &= \frac{(A_{16}+A_{26})}{W_2H},\\
\xi_5 &= \frac{2(B_{11}-B_{22})}{W_2H^2},\\
\xi_7 &= \frac{4(B_{16}+B_{26})}{W_2H^2},
\end{aligned}$$

with thermal material invariants [27] W and W^{th}

$$\begin{aligned}
W_2 &= \frac{1}{2}(Q_{11}-Q_{22}),\\
W_1^{th} &= \alpha_{11}Q_{11}+(\alpha_{11}+\alpha_{22})Q_{12}+\alpha_{22}Q_{22},\\
W_2^{th} &= \alpha_{11}Q_{11}+(\alpha_{22}-\alpha_{11})Q_{12}+\alpha_{22}Q_{22},
\end{aligned}$$

where H is the laminate thickness, α the coefficients of thermal expansion, and Q the reduced ply stiffness.

2.3 Equilibrium and Stability Analysis

Equilibrium configurations of the anisotropic tape spring in the twisting domain are identified by stationary points of the strain energy, *i.e.*,

$$\begin{aligned}
\frac{\partial U}{\partial \theta} &= \frac{C}{4R}(\lambda_1\sin(2\theta)+\lambda_2\cos(2\theta)...\\
&\quad +\lambda_3\sin(4\theta)+\lambda_4\cos(4\theta))=0,
\end{aligned} \tag{10}$$

$$\begin{aligned}
\frac{\partial U}{\partial C} &= \frac{1}{R}(\phi_1+\phi_2\cos^2(\theta)+\phi_3\cos^4(\theta)+\phi_4\sin(2\theta)...\\
&\quad +\phi_5\sin^2(2\theta)+\frac{\lambda_4}{2}\sin(2\theta)\cos^2(\theta))=0,
\end{aligned} \tag{11}$$

where

$$\begin{aligned}
\lambda_1 &= 4(D_{22}^*-D_{12}^*)+2CR(D_{11}^*-D_{22}^*)...\\
&\quad +4R(\Delta\kappa_x^{th}(D_{12}^*-D_{11}^*)+\Delta\kappa_y^{th}(D_{22}^*-D_{12}^*)...\\
&\quad +\Delta\kappa_{xy}^{th}(D_{26}^*-D_{16}^*)),\\
\lambda_2 &= 4CR(D_{16}^*+D_{26}^*)-8R(\Delta\kappa_x^{th}D_{16}^*...\\
&\quad +(\Delta\kappa_y^{th}+1/R)D_{26}^*+\Delta\kappa_{xy}^{th}D_{66}^*),\\
\lambda_3 &= CR(4D_{66}^*+2D_{12}^*-D_{22}^*-D_{11}^*),\\
\lambda_4 &= 4CR(D_{26}^*-D_{16}^*),
\end{aligned}$$

and

$$
\begin{aligned}
\phi_1 &= CRD^*_{11} - D^*_{12} - R(D^*_{11}\Delta\kappa^{th}_x + D^*_{12}\Delta\kappa^{th}_y + D^*_{16}\Delta\kappa^{th}_{xy}),\\
\phi_2 &= (D^*_{12} - D^*_{22}) + 2CR(D^*_{12} - D^*_{11}) + R(\Delta\kappa_x(D^*_{11} - D^*_{12})...\\
&\quad + \Delta\kappa_y(D^*_{12} - D^*_{22}) + \Delta\kappa_{xy}(D^*_{16} - D^*_{26})),\\
\phi_3 &= CR(D^*_{11} + D^*_{22} - 2D^*_{12}),\\
\phi_4 &= 2CRD^*_{16} - D^*_{26} - R(D^*_{16}\Delta\kappa_x + D^*_{26}\Delta\kappa_y + D^*_{66}\Delta\kappa_{xy}),\\
\phi_5 &= CRD^*_{66}.
\end{aligned}
$$

See Equations 2 and 7 for definitions of $\mathbf{D}^*$ and $\Delta\boldsymbol{\kappa}^{th}$ terms respectively.

The Hessian matrix of the strain energy provides a stiffness matrix for the tape spring, with respect to generalised degrees of freedom θ and C. A negative determinant of the Hessian indicates that the system is unstable, as one of the eigenvalues is negative. Conversely, a positive determinant indicates a stable system. The determinant of the Hessian matrix is,

$$
\begin{aligned}
|\mathbf{H}(U)| &= \begin{vmatrix} \frac{\partial^2 U}{\partial\theta^2} & \frac{\partial^2 U}{\partial\theta\partial C} \\ \frac{\partial^2 U}{\partial\theta\partial C} & \frac{\partial^2 U}{\partial C^2} \end{vmatrix}...\\
&= \frac{\partial^2 U}{\partial\theta^2}\frac{\partial^2 U}{\partial C^2} - \frac{\partial^2 U}{\partial\theta\partial C}\frac{\partial^2 U}{\partial C\partial\theta},
\end{aligned}
\tag{12}
$$

where the individual terms are,

$$
\begin{aligned}
\frac{\partial^2 U}{\partial\theta^2} &= \frac{C}{2R}(\lambda_1\cos(2\theta) - \lambda_2\sin(2\theta)...\\
&\quad + 2\lambda_3\cos(4\theta) - 2\lambda_4\sin(4\theta))
\end{aligned}
\tag{13}
$$

$$
\begin{aligned}
\frac{\partial^2 U}{\partial C^2} &= D^*_{11} + 2D^*_{16}\sin(2\theta) + D^*_{66}\sin^2(2\theta)...\\
&\quad + \psi_1\cos^2(\theta) + \psi_2\cos^4(\theta)...\\
&\quad + \psi_3\sin(2\theta)\cos^2(\theta)
\end{aligned}
\tag{14}
$$

$$
\begin{aligned}
\frac{\partial^2 U}{\partial\theta\partial C} &= \frac{1}{2R}(\lambda_5\sin(2\theta) + \lambda_6\cos(2\theta)...\\
&\quad + \lambda_3\sin(4\theta) + \lambda_4\cos(4\theta),
\end{aligned}
\tag{15}
$$

with

$$
\begin{aligned}
\psi_1 &= 2(D^*_{12} - D^*_{11})\\
\psi_2 &= \frac{\phi_3}{CR}\\
\psi_3 &= \frac{\lambda_4}{2CR}
\end{aligned}
$$

and

$$
\begin{aligned}
\lambda_5 &= 2(D^*_{22} - D^*_{12}) + 2CR(D^*_{11} - D^*_{22})...\\
&\quad + 2R(\Delta\kappa^{th}_x(D^*_{12} - D^*_{11}) + \Delta\kappa^{th}_y(D^*_{22} - D^*_{12})...\\
&\quad + \Delta\kappa^{th}_{xy}(D^*_{26} - D^*_{16})),\\
\lambda_6 &= 4CR(D^*_{16} + D^*_{26}) - 4R(\Delta\kappa^{th}_x D^*_{16}...\\
&\quad + (\Delta\kappa^{th}_y + 1/R)D^*_{26} + \Delta\kappa^{th}_{xy}D^*_{66}).
\end{aligned}
$$

Table 2: Predicted equilibrium states

Figure 2a			Figure 2b			Figure 2c		
Curvature (mm^{-1})	Twist Angle θ (°)	Stability $\lvert\mathbf{H}(U)\rvert$	Curvature (mm^{-1})	Twist Angle θ (°)	Stability $\lvert\mathbf{H}(U)\rvert$	Curvature (mm^{-1})	Twist Angle θ (°)	Stability $\lvert\mathbf{H}(U)\rvert$
1.11	90.0	-11.7	8.58	90.0	-56.4	8.58	91.3	-56.3
26.3	0.0	77.6	18.8	0.0	-19.8	18.8	1.8	-19.5
-	-	-	20.8	21.9	37.4	20.4	21.9	33.9
-	-	-	20.8	158.0	38.2	21.2	158.2	59.2

Table 2 details the equilibrium conditions predicted for the $[90_2/0_2]$ tape spring in Figure 2. Initial guesses for the equilibria were identified via visual inspection of the energy landscapes, and the equations were then solved numerically using the MATLAB function `fsolve`.

A zero-stiffness structure will exhibit no change in internal strain energy U throughout the designed mode of deformation (*i.e.* θ or C), and will thus be in constant equilibrium and thus be neutrally stable for all desired deformations. Guest *et al.* [5] describe a zero torsional stiffness tape spring using an isotropic material and mechanically introduced prestress. For prestressed composite tape springs the system is governed by coupled nonlinear equations for $\partial U/\partial\theta = 0$ and $\partial^2 U/\partial\theta^2 = 0$, even when simplified for cross-ply laminates where $D^*_{16} = D^*_{26} = 0$. A full exploration of the design space, in terms of material selection, lay-up and manufacturability, has not yet been attempted and is beyond the scope of the current investigation. Alternatively, multiple laminates could be used together to achieve overall mechanism zero-stiffness (for example like previous work by Murphey and Pellegrino [7]), although this comes at the cost of increased manufacturing complexity. Other mechanism geometries, prestressing techniques and constituent materials may yield zero-stiffness responses more easily, but these lie outside the scope of this work.

2.4 Energy Landscape Comparisons

In order to illustrate the effects of including thermal pre-stress a comparison of the energetic landscapes are presented. Figure 2 shows polar plots of non-dimensional strain energy $\hat{U}$ as a function of tape spring twist, 2θ, and underlying cylinder curvature, C. The tape spring is a $[90_2/0_2]$ IM7-8552 composite laminate shell with a manufactured radius of 38 mm. A $\Delta T = -155$°C models the cool down from a typical 180°C cure to room temperature. Figure 2a shows the energy landscape for a cross-ply tape spring with no thermal prestress: it is monostable with a low energy ($\hat{U}$<0.1) twisting region of approximately ± 20°. The low energy twist behaviour is due to the open cross-section of the tape spring. Figure 2b shows the effect of a thermally-induced prestress: the structure becomes bistable, with an unstable zero twist configuration (i.e. no equilibrium when the $C = 1/R$). The low-energy twisting region increases to approximately ± 45°, illustrating the potential for using thermal prestress to reduce the torsional stiffness of thin shell composite structures. Figure 2c shows the effect of fibre misalignment on the thermally prestressed shells. A misalignment of 2° in the inner two plies causes a slight rotation of the energy landscape; as a result, the manufactured configuration ($\theta = 0$) is no longer in equilibrium, and the structure will favour one twisted mode. While the energy landscape is different, the location of equilibria and the range of the low energy twisting region are similar to the non-misaligned tape spring.

3 Finite Element Model

3.1 Modelling Approach

To support the results from the analytical energy landscapes, Finite Element (FE) analyses were conducted in Abaqus/Standard 2016. The tape springs were meshed using S4R shell elements. A mesh refinement study compared the cross-sectional curvature at the centre of the post-warped, untwisted tape springs. Mesh target sizes of between 8×8 mm and 1×1 mm were considered, and a final mesh size of 5×5 mm was selected, as the calculated curvature converged to within 0.10% of the analysis with a 1×1 mm mesh density. A fully-fixed boundary condition was applied to the central node, and general geometrically nonlinear static analyses were conducted. The post-cure cooling process which generates the thermal prestress and resulting warp was modelled by applying two ambient temperature fields to the entire tape spring as 'Predefined Field' variables. The two temperatures modelled were (i) the expected cure temperature (180°C), and (ii) the assumed room temperature (25°C), to give $\Delta T = -155$°C. An example of the resulting deformed shape is shown in Figure 3a. For each model the deformed nodal coordinates were exported as a point cloud so that the tape spring twist angle and radius of underlying cylinder could be measured.

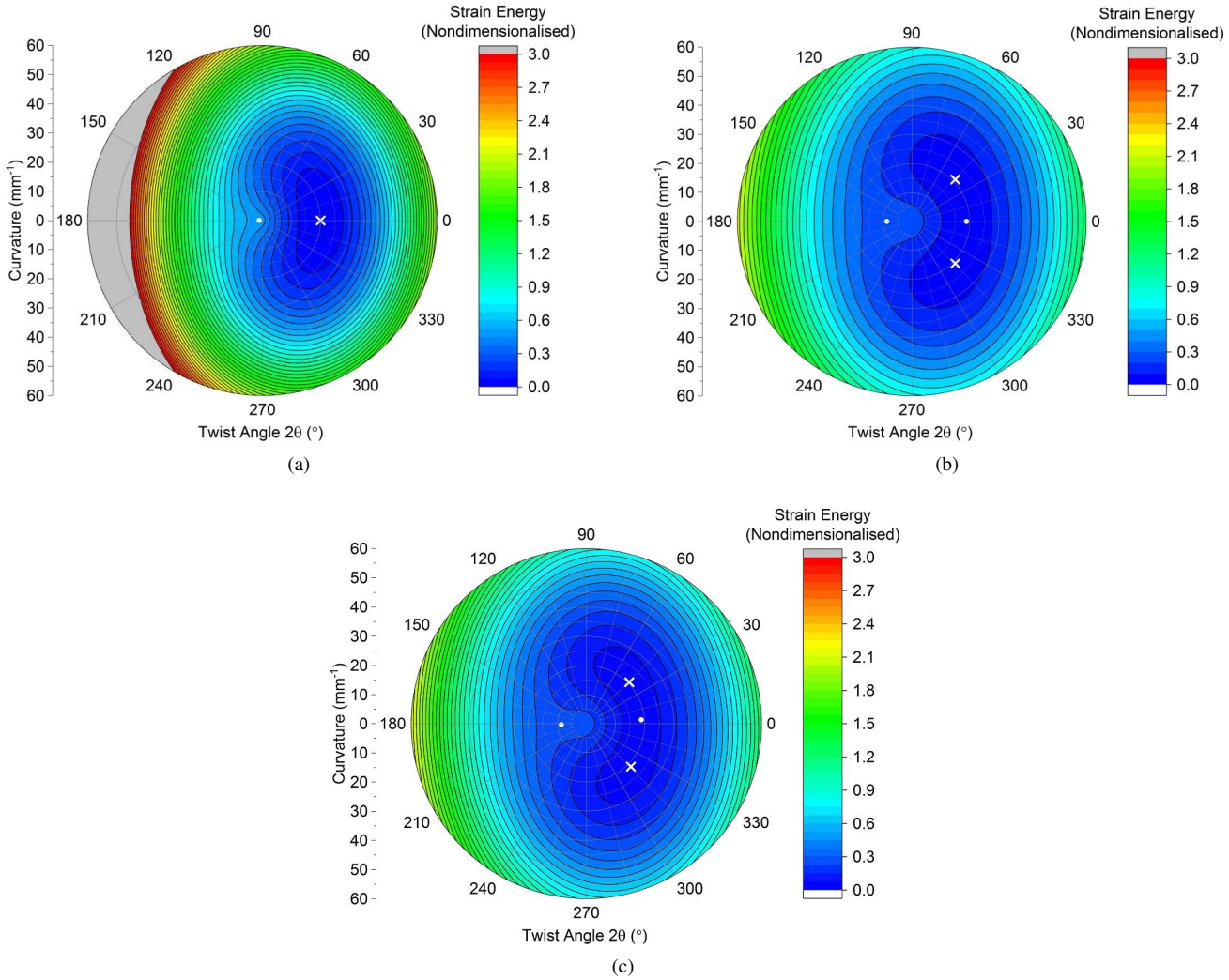

Fig. 2: Polar plots of nondimensional energy $\hat{U}$ as a function of tape spring twist, 2θ, on the angular axis and cylinder curvature, C, on the radial axis. Contours are plotted for $\hat{U}$ values between 0.0 to 3.0 inclusive with intervals of 0.1. (a) shows the landscape for a $[90_2/0_2]$ tape spring with manufactured radius $R = 38$ mm with no thermal prestress; (b) shows the landscape for a thermally prestressed tape spring; and (c) shows the same landscape as (b), but for a misaligned layup of $[88_2/0_2]$. Points labelled with a cross indicate the stable state(s), and dots indicate unstable equilibria.

3.2 Twisted Configurations

The warped shape shown in Figure 3a exists in a zero-twist configuration. The curling effects seen at the ends are due to residual moments from the thermal prestress. A prestressed $[90_N/0_N]$ cross-ply tape spring in this configuration corresponds to the unstable zero-twist equilibrium point in Figure 2b. The model possesses geometric and material symmetry, and thus cannot automatically bifurcate to a twisted configuration. In order to break this symmetry and let the model bifurcate to a preferred stable configuration, a small fibre misalignment was applied to each 90° ply in the laminate until a twisted structure was produced (-2° for the 38 mm radius springs; -5° for the 50 mm radius spring). Energy landscapes of tape springs with fibre misalignment (see example Figure 2c) were considered sufficiently similar to those without (see Table 2), that direct comparisons could be drawn between the 'misaligned' FE models and the other investigative approaches. An example twisted structure prediction can be seen in Figure 3b.

4 Prototype Manufacture

4.1 Design Curvature

The upper limit on the manufactured radius R is determined by the requirement that the warped tape spring nominally conforms to a cylindrical configuration. This is violated when the calculated thermally induced curvature $\Delta\kappa_y^{th}$ is equal to the manufacturing tooling curvature $1/R$. For an IM7-6552 [90/0] cross-ply laminate, this equates to a tooling radius of

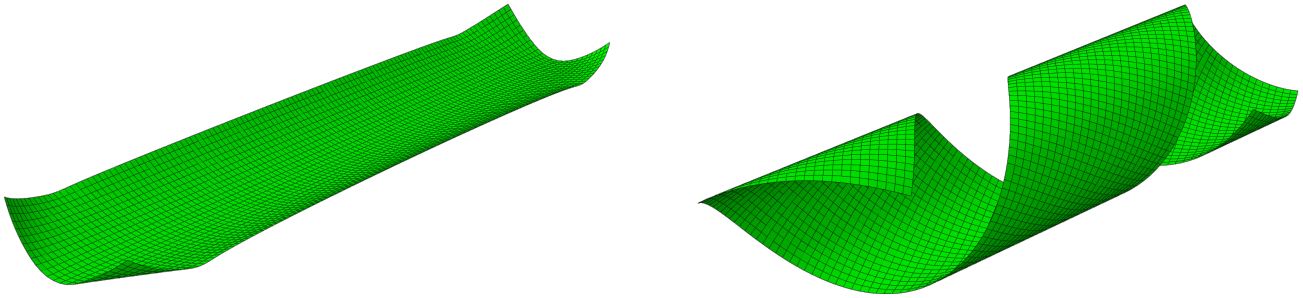

(a) (b)

Fig. 3: FE predictions of (a) the unstable untwisted post-warp shape, and (b) the stable twisted shape for a [90/0] layup with tool radius $R = 38$ mm.

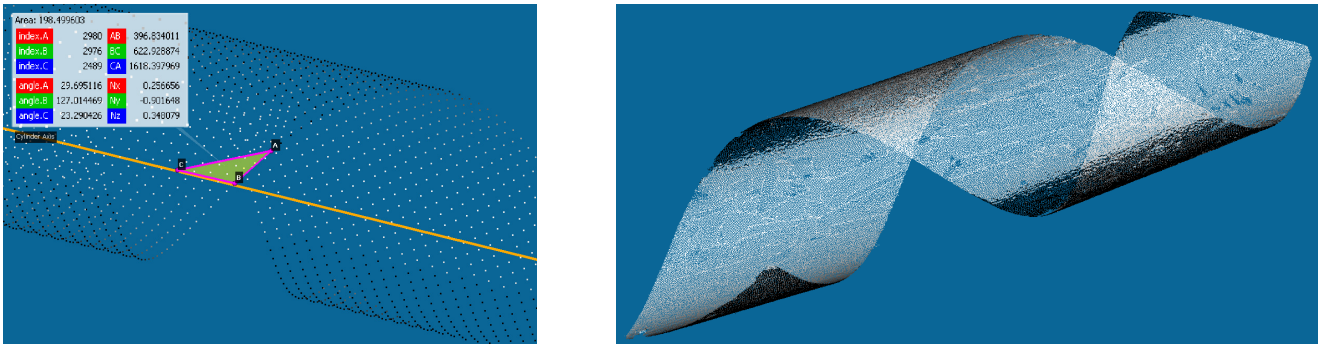

(a) (b)

Fig. 4: Images of (a) twist angle measurement using a cloud of FE nodal positions and the underlying cylinder axis, and (b) the point cloud from the laser scan of sample R38T1

approximately 55 mm, and represents the limit at which the warped tape spring is cylindrical (and the analytical model is valid). Therefore, steel tooling of radius 38 mm and 50 mm was selected for ply layup to ensure that manufactured tape springs were within this limit. A naming convention of the form *RXXTN* describes each sample, where *XX* refers to the manufactured tool radius (mm) and *N* refers to the layup $[90_N/0_N]$.

4.2 Manufacturing Process

A manual layup and vacuum-bagging process was used before curing the samples in an autoclave. Plies of pre-impregnated (prepreg) carbon fibre (IM7-8552) were laid-down to create rectangular plates with a $[90_N/0_N]$ layup. The resulting laminates were placed on steel tubes to provide the design curvature, with the 0° fibre direction aligned with the tube cylindrical axis. The inner 90° plies were separated from the tool surface by a layer of release film. A heat gun was used periodically to increase the prepreg tackiness and encourage adhesion to the tool surface. Once the layup was complete, an envelope bag was constructed around the tube, and a vacuum was applied to consolidate the plies on the tool. The samples were cured at 7 bar pressure and 180°C in an autoclave. The cured tape springs were allowed to cool down to ambient temperature before being released from their vacuum bags (to minimise moisture uptake from the atmosphere that could affect twisted geometry). Once cooled, the samples were de-bagged and mass readings were immediately taken to establish a nominally zero-moisture benchmark, and geometric measurements were conducted within 24 hours.

4.3 Profile Measurement

The geometric information of the shell mechanisms was recorded using a FARO Edge ScanArm® optical measurement device and associated CAM2 Measure 10.7 software. This device consists of a laser scanning probe mounted upon a moveable arm, and generates a 'cloud' of *XYZ* data points of complex geometries. Point clouds were also generated from the deformed nodal positions of the FE models, to enable comparison with the manufactured prototypes.

The first parameter used for validation was the helical twist angle, defined as the angle of orientation of the twisted

Table 3: Overall twist angles and underlying cylinder radii

	Manufacture			Helix Radius (mm)			Twist Angle (°)		
Sample	Layup	Radius (mm)	ΔT (°C)	Theory	FE	Experiment	Theory	FE	Experiment
R38T2	$[90_2/0_2]$	38	-162.7	48.1	50.6	50.9	22	21.8	16.9
R38T2 (+1 wk)	$[90_2/0_2]$	38	-162.7	48.1	-	47.4	22	-	6.0
R38T1	$[90/0]$	38	-163.9	48.1	47.3	55.5	55	53.0	47.8
R50T1	$[90/0]$	50	-164.6	63.3	-	80	87	-	90

shell with respect to the length-wise axis of an underlying cylinder. This angle was measured by analysing the sample point clouds using the software CloudCompare [28]; see Figure 4a. The second parameter, underlying curvature, is directly measured from a fitted cylinder. The same procedures were applied to both the experimentally measured point clouds and those extracted from the FE analysis. FE and experimental results for the same tape spring can be seen in Figure 3b and Figure 4b respectively. The difference in twist direction is due to the arbitrary choice of fibre angle misalignment direction in the FE model. After FE-predicted geometries and manufactured sample geometries had been recorded, comparisons could be made between all three approaches to verify the analytical energy landscapes.

5 Results & Discussion

Comparisons between the calculated stable twisted configurations, using the methodology from Section 2, and the measured twist angles and helix cylinder radii are presented in Table 3; the corresponding energy plots for each sample are shown in Figure 5. Experimental results for R50T1 were from visual inspection and not point cloud measurement due to the shell being almost completely coiled post-cure and thus impractical for laser scanning. Table 3 shows good agreement between the analytical and FE models for both twist angles (range within 2°) and helix radii (range within 3 mm), as well as with the experimental results. The discrepancies could be attributed to manufacturing sensitivity of thin-shell composites, a higher ΔT observed in the manufactured samples, as well moisture ingress between manufacture and measurement.

Interestingly, after one week the measured twist angle of the R38T2 sample reduced by approximately 65%. Figure 6b shows the manufactured R50T1 sample after a week-long exposure to the ambient environment: the reduction in twist angle (and extension in length) is clearly visible compared to Figure 6a. It is hypothesised this is due to viscoelastic relaxation and moisture ingress, and their 'relaxation' effects on thermal stresses [29, 30]. The relaxation is a short-term effect: bistable samples tended to favour one twist direction within hours (in contradiction to energy landscape predictions in Figure 5), potentially accentuating any fibre misalignment effects from manufacturing.

Storing samples in a desiccator will mitigate against moisture effects. Quantifying the degree of recovery from moisture effects, as well as the impact of moisture on design spaces remains the subject of ongoing investigation. While controlling temperature during manufacture is possible, controlling the usage temperature and ambient moisture is much more challenging. A composite compliant shell mechanism relying on thermal prestress will therefore behave differently depending on its environment conditions, and some degree of active thermal control may be necessary depending on the application and required mechanical responses.

Finally, it was possible to induce non-cylindrical stable shapes with R50T1 by manually twisting and buckling the sample. One such stable configuration can be seen in Figure 6c, and highlights the limitations of assuming that the underlying deformed shell structure is cylindrical. If a general approach for designing composite compliant shells is to be realised, then a less geometrically-restrictive model is required.

6 Conclusions

In conclusion, making use of the residual stresses in a cross-ply composite cylindrical shell has been shown to increase the range of twist angles that can be achieved at low ($\hat{U} \leq 0.1$) levels of internal strain energy. This demonstrates the potential of using anisotropy in composite materials to tailor the stiffness of compliant mechanisms in ways not available to isotropic materials. Furthermore it illustrates the potentially significant changes in geometry and behaviour that can occur in thermally-prestressed thin composite shells, and the importance of incorporating thermal effects into the design and analysis of compliant or multistable structures. An extension of an existing composite tape spring model [4] incorporating thermal effects has been presented, as well as finite element simulations and experimental samples of tape springs of different thickness and manufactured radius. All approaches were shown to have good agreement in predicting the tape spring twisted

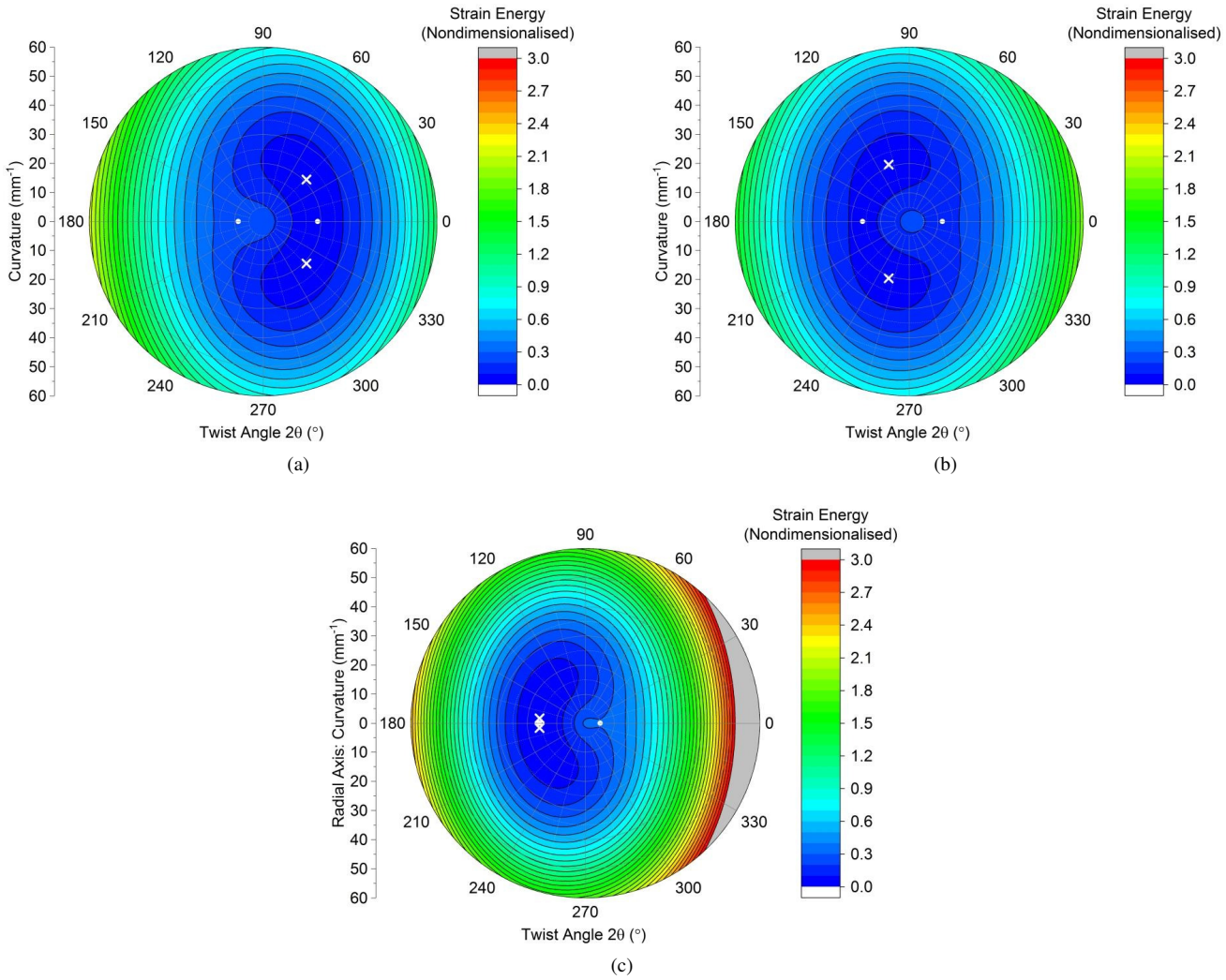

Fig. 5: Polar plots of nondimensional energy $\hat{U}$ as a function of tape spring twist, 2θ, on the angular axis and cylinder curvature, C, on the radial axis. Contours are plotted for $\hat{U}$ values between 0.0 to 3.0 inclusive with intervals of 0.1. Subfigures show (a) R38T2, (b) R38T1, and (c) R50T1. All predict unstable on-tool configurations, with (a) and (b) being clear bistable twisted structures, and (c) almost a monostable coiled structure. Points indicated by a cross represent stable state(s) and dots indicate unstable equilibria.

states. Very good agreement for helical twist angle and radius was shown between theoretical and FE predictions, with experimental results indicating that these structures are sensitive to manufacturing variations.

The feasibility of a composite tape spring with zero torsional stiffness has also been explored. A zero torsional stiffness tape spring system has been shown to be governed by a set of coupled nonlinear equations, even for cross-ply laminates where D^*_{16} and D^*_{26} effects are removed. Further work is required to explore these coupled equations and more generally quantify the limits of stiffness reduction achievable using thermal prestress.

Several other design-influencing factors have been identified, including temperature control, viscoelastic effects, moisture-driven behaviour changes and experimental measurement methods. These factors must be addressed for a practical thermally prestressed composite shell to be realised, and each presents interesting avenues for further study. Future areas of work include refinement of measurement methods, measuring shape recovery by drying samples, and investigations into any long term viscoelastic relaxation.

Data Access Statement

All data necessary to support the conclusions are provided within the paper.

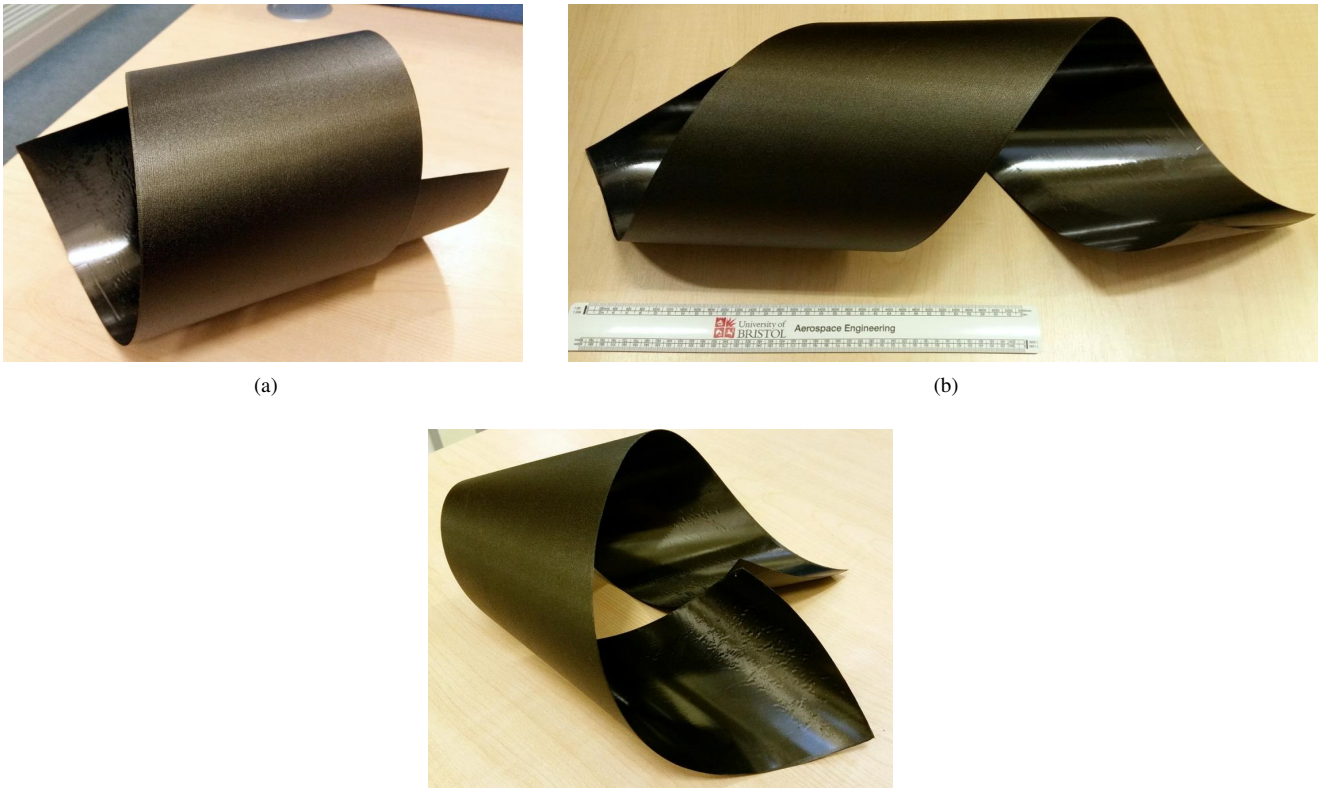

(a) (b)

(c)

Fig. 6: Photos of sample R50T1 showing: (a) its original monostable configuration, (b) the extended monostable configuration, and (c) an example of a stable configuration not predicted by either model

Acknowledgements

The work detailed in this paper was funded by the Engineering and Physical Sciences Research Council (EPSRC) as part of the Centre for Doctoral Training in Advanced Composites for Innovation and Science (grant number EP/L016028/1). The authors also wish to thank Prof. Just Herder, Werner van de Sande and Giuseppe Radaelli (TU Delft) for their support and helpful discussions about compliant mechanisms, as well as Boudewijn Wisse (Laevo BV) for sharing his insights into compliant mechanism technology in exoskeletons.

References

[1] Radaelli, G., and Herder, J., 2014. "Isogeometric Shape Optimization for Compliant Mechanisms With Prescribed Load Paths". In Proc. ASME 2014 IDETC/CIE.

[2] Radaelli, G., and Herder, J., 2016. "A monolithic compliant large-range gravity balancer". *Mech. Mach. Theory,* **102**, aug, pp. 55–67.

[3] Weaver, P., O'Donnell, M., and York, C., 2010. "Approximations for Warp-Free Laminate Configurations". In 51st AIAA/ASME/ASCE/AHS/ASC Struct. Struct. Dyn. Mater. Conf. 18th AIAA/ASME/AHS Adapt. Struct. Conf.

[4] Guest, S., and Pellegrino, S., 2006. "Analytical models for bistable cylindrical shells". *Proc. R. Soc. A Math. Phys. Eng. Sci.,* **462**(2067), mar, pp. 839–854.

[5] Guest, S., Kebadze, E., and Pellegrino, S., 2011. "A zero-stiffness elastic shell structure". *J. Mech. Mater. Struct.,* **6**(1-4), jun, pp. 203–212.

[6] Seffen, K., and Guest, S., 2011. "Prestressed Morphing Bistable and Neutrally Stable Shells". *J. Appl. Mech.,* **78**(1), p. 011002.

[7] Murphey, T., and Pellegrino, S., 2004. "A Novel Actuated Composite Tape-Spring for Deployable Structures". In 45th AIAA/ASME/ASCE/AHS/ASC Struct. Struct. Dyn. Mater. Conf.

[8] Schultz, M., Hulse, M., Keller, P., and Turse, D., 2008. "Neutrally stable behavior in fiber-reinforced composite tape springs". *Compos. Part A Appl. Sci. Manuf.,* **39**(6), pp. 1012–1017.

[9] Morsch, F., and Herder, J., 2010. "Design of a Generic Zero Stiffness Compliant Joint". In Proc. ASME 2010 IDETC/CIE.

[10] Herder, J., Barents, R., Schenk, M., van Dorsser, W., and Wisse, B., 2011. "Spring-to-Spring Balancing as Energy-Free Adjustment Method in Gravity Equilibrators". *J. Mech. Des.,* **133**(June 2011), p. 061010.

[11] Schenk, M., and Guest, S., 2014. "On zero stiffness". *Proc. Inst. Mech. Eng. Part C J. Mech. Eng. Sci.,* **228**(10), pp. 1701–1714.

[12] Cantera, M., Romera, J., Adarraga, I., and Mujika, F., 2014. "Modelling of [0/90] laminates subject to thermal effects considering mechanical curvature and through-the-thickness strain". *Compos. Struct.,* **110**(1), apr, pp. 77–87.

[13] Nettles, A., 1994. Basic mechanics of laminated composite plates. Tech. Rep. October 1994, NASA Marshall Space-flight Centre.

[14] Mansfield, E., 1989. *The Bending & Stretching of Plates*, 2nd ed. Cambridge University Press.

[15] Daynes, S., and Weaver, P., 2013. "Stiffness tailoring using prestress in adaptive composite structures". *Compos. Struct.,* **106**, pp. 282–287.

[16] Pirrera, A., Lachenal, X., Daynes, S., Weaver, P., and Chenchiah, I., 2013. "Multi-stable cylindrical lattices". *J. Mech. Phys. Solids,* **61**(11), pp. 2087–2107.

[17] Lachenal, X., Weaver, P., and Daynes, S., 2012. "Multi-stable composite twisting structure for morphing applications". *Proc. R. Soc. A Math. Phys. Eng. Sci.,* **468**(2141), pp. 1230–1251.

[18] Lachenal, X., Daynes, S., and Weaver, P., 2013. "A zero torsional stiffness twist morphing blade as a wind turbine load alleviation device". *Smart Mater. Struct.,* **22**(6), p. 065016.

[19] Fancey, K., and Pang, J., 2009. "The flexural stiffness characteristics of viscoelastically prestressed polymeric matrix composites". *Compos. Part A Appl. Sci. Manuf.,* **40**(6-7), pp. 784–790.

[20] Brinkmeyer, A., Pellegrino, S., and Weaver, P., 2015. "Effects of Long-Term Stowage on the Deployment of Bistable Tape Springs". *J. Appl. Mech.,* **83**(1), nov, p. 011008.

[21] Fancey, K., and Fazal, A., 2016. "Prestressed polymeric matrix composites: Longevity aspects". *Polym. Compos.,* **37**(7), jul, pp. 2092–2097.

[22] Nijssen, J., 2016. "A Type Synthesis Approach to Compliant Shell Mechanisms". Application, Delft University of Technology.

[23] Murphey, T., Francis, W., Davis, B., and Mejia-Ariza, J., 2015. "High Strain Composites". In 2nd AIAA Spacecr. Struct. Conf.

[24] Ratcliffe, J., Czabaj, M., and O'Brien, T., 2012. "Characterizing Delamination Migration in Carbon/Epoxy Tape Laminates". In 27th Am. Soc. Compos. Tech. Conf.

[25] Weaver, P., 2005. "Anisotropic Laminates That Resist Warping During Manufacture". In ICCM15 - 15th Int. Conf. Compos. Mater.

[26] Diaconu, C., and Sekine, H., 2004. "Erratum on Flexural Characteristics and Layup Optimization of Laminated Composite Plates Under Hygrothermal Conditions Using Lamination Parameters". *J. Therm. Stress.,* **27**(12), dec, pp. 1213–1216.

[27] Tsai, S., 1981. *Introduction to Composite Materials*. Technomic Publishing, Westport, CT.

[28] Girardeau-Montaut, D. CloudCompare Project. http://www.danielgm.net/cc/.

[29] Etches, J., Potter, K., Weaver, P., and Bond, I., 2009. "Environmental effects on thermally induced multistability in unsymmetric composite laminates". *Compos. Part A Appl. Sci. Manuf.,* **40**(8), pp. 1240–1247.

[30] Telford, R., 2014. "Hygro-thermal Residual Stresses in Unsymmetrical Multi-Stable Composite Laminates". PhD thesis, University of Limerick.